Automatic detection and segmentation of colonic polyps in wireless capsule images

Isabel N. Figueiredo* Surya Prasath* Yen-Hsi R. Tsai† Pedro N. Figueiredo‡

September 22, 2010

Abstract

In this paper we address the problem of detection and segmentation of colonic polyps in endoscopic images obtained by a capsule device. Several procedures based on the geometric and image intensity features of the input medical image, together with variational segmentation methods are proposed and analyzed. The most successful procedure, and which has proven to efficiently detect and single out the colonic polyps, relies on the curvature information of the images, which are interpreted as the graphs of functions defined over the pixel domain. The procedure involves first a curvature based identification to the graph of the original input image, and then a variational segmentation relying on this curvature identification. The other procedures are "image intensity" based segmentation techniques, and lead to a good detection of the lumen and colonic mucosa. However, in the majority of the cases, and as opposed to the first procedure, these "image intensity" based techniques do not single out the polyp, they rather include it as a part of the colonic mucosa segmentation. Numerical experiments on wireless capsule endoscopic images are undertaken for evaluation and validation of the proposed approaches.

1 Introduction and motivation

Wireless capsule endoscopy is a new imaging modality in gastroenterology, which acquires digital photographs of the intestine tract using a swallowable miniature camera device with LED flash lights [1, 8, 12, 15, 16, 17, 18]. The capsule wirelessly transmits images of the gastrointestinal tract to a portable recording device. The captured images are then analyzed by medical doctors (gastroenterologists), who should locate and detect abnormal features or lesions, and carry out diagnostic assessments. A capsule can record more than 50,000 images, during its operation time, which spans a duration of 8 to 10 hours. Hence, the process of examining each image sequence produced by a capsule is an extremely time consuming process. Clearly an efficient and accurate automatic detection procedure would relieve the diagnosticians of the burden of analyzing a large number of images for each patient.

In this paper we focus on images produced by the PillCam Colon capsule (see Figure 1). This device, released in 2006, was specifically developed for colon visualization and also with the purpose of screening for colorectal cancer, as an alternative to conventional colonoscopy. By imaging the colon in a sequential way, the capsule images can help in early cancer detection. The primary objective in this paper is to automatically detect and segment polyps in images captured with this colon capsule.

The polyps to be detected in the images are characterized by physicians according to human perception of their distinctive shapes, and also in some cases, by their color and texture on these geometric objects. In effect, according to medical information the geometry of colonic polyps can be classified essentially in two types: pedunculate polyps, which are mushroom-like structures attached by a thin stalk to the colon

*CMUC, Department of Mathematics, University of Coimbra, 3001-454 Coimbra, Portugal.

†Department of Mathematics, University of Texas at Austin, Austin, TX 78712, USA.

‡Faculty of Medicine, University of Coimbra, 3004-504 Coimbra, and Department of Gastroenterology, University Hospital of Coimbra, 3000-075 Coimbra, Portugal.

mucosa, and sessile polyps, which are like caps (mushroom structures with no stalk). Their color is in general red, reddish or rose, and their texture can be very similar to a human brain.

In this paper we mainly explore the geometry features of colonic polyps and derive a suitable procedure to detect and segment them. In particular those with no peduncle appear to take locally convex shape which resembles the cap of a mushroom. This geometrical identification of colonic polyps is translated in terms of the Gaussian and mean curvatures of the graph of an input (smoothed out) gray-scale image. From the two curvatures, we define a new "image" which attains relatively large positive values in possible polyps locations and relative small values in other regions in a given image. Later in the paper, we shall demonstrate that this procedure singles out correctly the location of colonic polyps and leads to a good segmentation of the visible portion of the polyps.

Since the images acquired by the PillCam capsule are basically photographs of the colon interior with lighting source in the viewing direction, it is natural to perform our geometric identification of polyps on surfaces that are reconstructed from the capsule images. Indeed, we have attempted apply some shape from shading algorithms (as described in [25, 28, 29]) to the original input images in order to obtain surfaces which approximate the colon interior. From these reconstructed surfaces, we applied our geometric identification. But from all images that we have tried, the reconstructed surfaces were very similar to the original images, interpreted as the graph of a scalar function of two variables (the pixel domain). Thus, finally, we decided to use the curvature based identification to the graph of the original image.

In addition, we also examine the "image intensity" properties of the input image, and propose segmentation methods for capsule endoscopy images. We apply variational segmentation methods, which rely on Chan and Vese model [5], with the modifications described in [11] (see also [10] for a related work). This choice is motivated by the good results we achieved with these methods, for *in vivo* colonic aberrant crypt foci, in endoscopic images acquired with a traditional endoscope (see [11]). To infer segmentation results from the "image intensity", we used a vector-valued variational segmentation model involving the three color channels (R,G,B) or a four-phase variational segmentation model (in one case, we also used a combination of the four-phase segmentation of the image intensity with a two-phase segmentation of the Gaussian curvature of the graph to the smoothed gray-scale input image). These "image intensity" approaches successfully detect the lumen and colonic mucosa (in particular the four-phase model performs better than the vector-valued model), but in the majority of the cases they do not isolate explicitly and clearly the colonic polyps. They rather include it as a part of the colonic mucosa segmentation.

Many recent studies have focused on detecting polyps on colonoscopy images (not capsule endoscopic images), as for example [7, 14, 30], and on analyzing capsule videos for other purposes, as for instance [2, 22]. Also several shape based schemes were proposed to find polyps in virtual colonoscopy or computed tomography colonography and have been addressed; see e.g. [13, 21, 23, 26, 31]. These methods take the already reconstructed surface representing the colon's interior. In contrast, ours comes from a simple photographic device, susceptible of having a lot of noise and restriction from lighting. Moreover, segmenting polyps from wireless capsule endoscopic images has not been considered so far, to the best of our knowledge, and none of the variational segmentation procedures and methods proposed in this paper was addressed for capsule endoscopic images. Neither have variational segmentations involving gaussian and mean curvatures, of the graph to the smoothed gray-scale input image, been reported in the literature. The results presented in the numerical experiments section demonstrate the efficacy of our proposed methods.

The plan of this paper is as follows. After this introduction, section 2 describes the models and numerical approximations used in this paper: the Gaussian and mean curvature computations in 2.1, and the variational segmentation methods in 2.2. In section 3 the results for several wireless endoscopic images are reported, and detailed discussion is included with respect to polyp segmentation and detection. Finally, section 4 concludes this paper, summarizing the main results and outlining future work.

(a)

(b)

(c)

Figure 1: Wireless capsule endoscopic device. (a) PillCam Colon capsule (size: 31×11 mm, distributor: *Given Imaging*, Yoqneam, Israel). Second row, examples of medical images obtained with the capsule: (b) from RAPID 6 Atlas v3 of *Given Imaging*, and (c) from Department of Gastroenterology, University Hospital of Coimbra.

2 The models and approximations

In this section we introduce the definition of the Gaussian and mean curvatures, explain how we compute them using a finite difference scheme, and provide some examples to test the accuracy of these approximations, as well as, their suitability for detecting colonic polyps in wireless capsule images. Finally, we give a quick summary of the variational segmentation methods applied in the paper.

2.1 Gaussian and mean curvatures

Let Ω be an open subset of $\mathbb{R}^2$, (x, y) an arbitrary point in Ω, and $u : \Omega \mapsto \mathbb{R}$ a twice continuously differentiable function. Then the Gaussian curvature $\mathcal{K}$ and the mean curvature $\mathcal{H}$ of the surface $S := \{(x, y, u(x, y)) : (x, y) \in \Omega\}$ are

$$\begin{aligned} \mathcal{K}(x,y) &:= \frac{u_{xx}u_{yy} - u_{xy}^2}{(1+u_x^2+u_y^2)^2}(x,y) \\ \mathcal{H}(x,y) &:= \frac{(1+u_{xx})^2 u_{yy} - 2u_x u_y u_{xy} + (1+u_{yy})^2 u_{xx}}{2\sqrt{(1+u_x^2+u_y^2)^3}}(x,y) \end{aligned} \tag{1}$$

where u_x, u_y and u_{xx}, u_{yy}, u_{xy} are first and second order partial derivatives of u with respect to x and y.

Our basic assumption is that a polyp can be identified as a convex protrusion of a relatively small size on the colon surface. Thus, we expect that the Gaussian curvature of a polyp surface to be relative higher than those of other regions, which may be either flat or ridge-like (folds). However, the Gaussian curvature does not distinguish concavity of the graph of u (protrusion) from convexity (depression), so we need additional information for such distinction. For this purpose, we decide to rely on the mean curvature of the graph of u, and from it we create a cut-off function which filters out the convex part of the graph. We propose to use the function

$$\mathcal{P} := -\mathcal{K}\min(\mathcal{H}, 0) \tag{2}$$

to identify potential polyps in the given images. $\mathcal{P}$ would yield relatively large positive values over polyps which match our assumptions. Figure 2 serves as a proof of concept for our proposed method involving

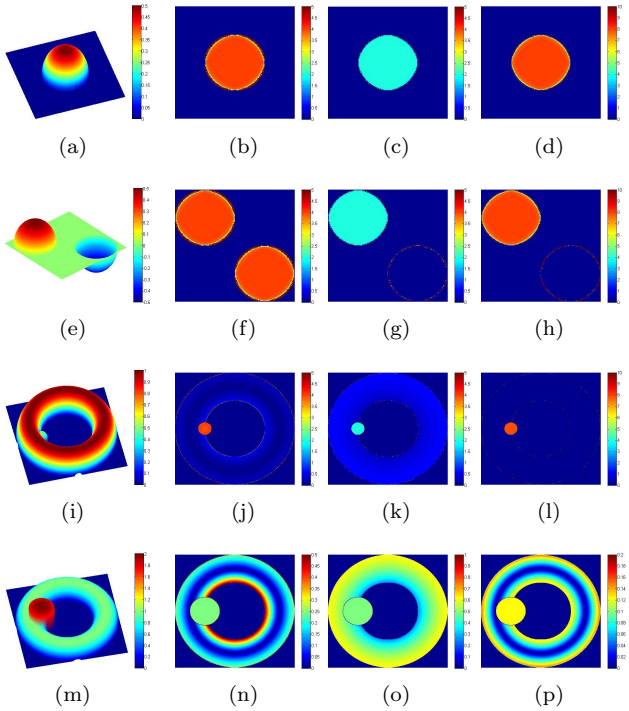

Figure 2: First column: Synthetic structures (emulating colonic folds and polyps). Second column: Gaussian curvatures. Third column: $-\min(\mathcal{H}, 0)$. Fourth column: $\mathcal{P} = -\mathcal{K}\min(\mathcal{H}, 0)$.

$\mathcal{K}$, $\mathcal{H}$ and $\mathcal{P}$ defined above for detecting polyps exhibiting a cap-like shape. It also illustrates the accuracy of this finite difference approximation scheme. In the first columns, four synthetic surfaces are depicted. In the second column, the Gaussian curvatures of each of the surfaces are depicted. The third column shows the corresponding values of the negative parts of the mean curvature. The last columns depicts the values of $\mathcal{P}$ for each of the surfaces.

Finally, as in the typical settings of PDE base image processing, we regard a given gray scale image as a grid function which samples the underlying scene over a rectangular domain Ω. Thus, we work with functions defined on Ω and then derive the corresponding formulas that can be applied to the given images on the pixel domain. Let now $(x_i, y_j) = (ih, jh)$, with $1 \leq i, j \leq M$ for some $h > 0$, be a Cartesian grid, defined in Ω. The function $u(x, y)$ correspond to the given image at continuum, and each pixel in the given image corresponds to a point $(x_i, y_j) = (ih, jh)$ on the grid. $u_{i,j}$ is then the image intensity of u at (x_i, y_j). The surface S mentioned above if thus the graph of the image function. We use the following standard centered differencing to approximate the partial derivatives that appear in the formulas for $\mathcal{K}$ and $\mathcal{H}$:

$$u_{x|(x_i,y_j)} \approx \frac{u_{i+1,j} - u_{i-1,j}}{2h}, \quad u_{y|(x_i,y_j)} \approx \frac{u_{i,j+1} - u_{i,j-1}}{2h},$$

and

$$u_{xx|(x_i,y_j)} \approx \frac{u_{i+1,j} - 2u_{i,j} + u_{i-1,j}}{h^2},$$

$$u_{yy|(x_i,y_j)} \approx \frac{u_{i,j+1} - 2u_{i,j} + u_{i,j-1}}{h^2},$$

and

$$u_{xy_{|u(x_i,y_j)}} \approx \frac{u_{i+1,j+1} - u_{i-1,j+1} - u_{i+1,j-1} + u_{i-1,j-1}}{4h^2}.$$

for the second derivatives. Furthermore, periodic boundary condition is assumed; i.e. $u_{M+1,j} = u_{1,j}$, $u_{-1,j} = u_{M,j}$, $u_{i,M+1} = u_{i,1}$, and $u_{i,-1} = u_{i,M}$.

2.2 Segmentation methods

Image segmentation is an image processing method, which consists in the partition of a given image into disjoint regions, representing distinct objects. Here we use 3 variational image segmentation models, which rely on the Chan and Vese model [5] and two extensions of it (the vector-valued and the multiphase segmentation models described in [4] and [27]), together with the modifications introduced in [11], with respect to the model definitions and their numerical solutions. The former includes two additional regularization terms. One is a Tikhonov like regularization term, and the other term penalizes deviations of the slope of the level set function from unity, and thus addresses the non-uniqueness of the level set function for a given shape. The numerical scheme involves a finite element discretization of the model weak variational formulation, followed by a Levenberg-Marquardt Newton-type optimization method for determining its solution. Our motivation, for this segmentation models choice, relies on the good results we have obtained with it, for *in vivo* colonic aberrant crypt foci, in endoscopic images, acquired with a traditional endoscope (see [11]).

We shortly describe now these variational models and refer on the particular numerical procedure for their solutions (a detailed description and justification of this scheme can be found in [11]). We emphasize that all the segmentation models described next are active contours without edges models, formulated by means of level set functions (see [19, 20]).

Let Ω be a bounded open set of $\mathbb{R}^2$, $I : \overline{\Omega} \longrightarrow \mathbb{R}^n$ be a given image (if $n > 1$ it is a vector-valued image). Each one of the models [5, 4, 27] is an optimization problem of the form

$$\min_{(\phi,c)} F(\phi, c) \tag{3}$$

where c is an unknown scalar vector representing the distinct regions in the image to be segmented, and ϕ is the (scalar or vectorial) function that represents the boundaries among these regions.

For the scalar model

$$\begin{aligned} & F(\phi, c) := \lambda^+ \textstyle\int_\Omega |I - c^+|^2 \, H(\phi)\, dx\, dy \\ + \quad & \lambda^- \textstyle\int_\Omega |I - c^-|^2 \, (1 - H(\phi))\, dx\, dy \\ + \quad & \mu \textstyle\int_\Omega \delta(\phi)|\nabla\phi|\, dx\, dy + \eta \int_\Omega H(\phi)\, dx\, dy \\ + \quad & \tfrac{\beta}{4} \textstyle\int_\Omega \left(|\nabla\phi|^2 - 1\right)^2 dx\, dy + \tfrac{\alpha}{2} \int_\Omega |\nabla\phi|^2\, dx\, dy. \end{aligned} \tag{4}$$

Here the given image I is a scalar function, the segmentation curve is represented by the zero level set of the scalar function $\phi : \Omega \longrightarrow \mathbb{R}$ and $c = (c^+, c^-)$, where c^+ and c^- are the averages of I, inside and outside, respectively, the segmentation curve. The function H is the Heaviside function ($H(z) := 1$ if $z \geq 0$, $H(z) := 0$ if $z < 0$), and $\delta(z) := \frac{d}{dz} H(z)$ is the Dirac delta function in the sense of distributions. The parameters $\lambda^+ > 0$, $\lambda^- > 0$, $\mu \geq 0$ and $\eta \geq 0$ are fixed : λ^+, λ^- are scale parameters weighting the fitting terms, μ is a regularizing parameter that penalizes the length of the boundaries (the term $\int_\Omega \delta(\phi(x,y))|\nabla\phi(x,y)|\, dx\, dy = \int_\Omega |\nabla H\big(\phi(x,y)\big)|\, dx\, dy$ just represents the length of the zero level set of ϕ, see [19]) and η is a regularizing parameter for the area inside the segmentation curve (this area is $\int_\Omega H(\phi(x,y))\, dx\, dy$). Finally, $\beta \geq 0$ and $\alpha \geq 0$ are two positive fixed parameters. The term $\frac{\beta}{4} \int_\Omega \left(|\nabla\phi|^2 - 1\right)^2 dx\, dy$ simply penalizes the deviation of the slope of the level set function from unity, which gives a well-defined level-set function (similarly to a signed distance function, which also attempts

to maintain a slope of 1). The term $\frac{\alpha}{2}\int_\Omega |\nabla\phi|^2\,dx\,dy$ is a Tikhonov like regularization (see [11]). In particular, the unknown averages c^+ and c^- are functions of ϕ given by

$$\begin{aligned} c^+(\phi) &= \frac{\int_\Omega I\,H(\phi)\,dx\,dy}{\int_\Omega H(\phi)\,dx\,dy}, \\ c^-(\phi) &= \frac{\int_\Omega I\,\big(1-H(\phi)\big)\,dx\,dy}{\int_\Omega \big(1-H(\phi)\big)\,dx\,dy}. \end{aligned} \tag{5}$$

For the vector-valued model

$$\begin{aligned} & F(\phi,c) := \int_\Omega \tfrac{1}{n}\textstyle\sum_{i=1}^n \lambda_i^+\,|I_i-c_i^+|^2\,H(\phi)\,dx\,dy \\ + \;& \int_\Omega \tfrac{1}{n}\textstyle\sum_{i=1}^n \lambda_i^-\,|I_i-c_i^-|^2\,(1-H(\phi))\,dx\,dy \\ + \;& \mu\int_\Omega \delta(\phi)|\nabla\phi|\,dx\,dy + \eta\int_\Omega H(\phi)\,dx\,dy \\ + \;& \tfrac{\beta}{4}\int_\Omega \big(|\nabla\phi|^2-1\big)^2\,dx\,dy + \tfrac{\alpha}{2}\int_\Omega |\nabla\phi|^2\,dx\,dy. \end{aligned} \tag{6}$$

Now the given image is a vector-valued function $I=(I_i)_{i=1}^n$, with $I:\overline{\Omega}\longrightarrow\mathbb{R}$, for $i=1,\dots,n$. The vector representing the averages of the image components (or channels) I_i is now $c=(c_i^+,c_i^-)_{i=1}^n$, and $(\lambda_i^+)_{i=1}^n$, $(\lambda_i^-)_{i=1}^n$ are the weighting parameters. The functions ϕ, H, δ and parameters μ, η, β and α have the same interpretation as before in (4).

For the four phase model

$$\begin{aligned} & F(\phi,c) := \lambda_{11}\int_\Omega |I-c_{11}|^2\,H(\phi_1)\,H(\phi_2)\,dx\,dy \\ + \;& \lambda_{10}\int_\Omega |I-c_{10}|^2\,H(\phi_1)\,\big(1-H(\phi_2)\big)\,dx\,dy \\ + \;& \lambda_{01}\int_\Omega |I-c_{01}|^2\,\big(1-H(\phi_1)\big)\,H(\phi_2)\,dx\,dy \\ + \;& \lambda_{00}\int_\Omega |I-c_{00}|^2\,\big(1-H(\phi_1)\big)\,\big(1-H(\phi_2)\big)\,dx\,dy \\ + \;& \mu_1\int_\Omega \delta(\phi_1)|\nabla\phi_1|\,dx\,dy + \eta_1\int_\Omega H(\phi_1)\,dx\,dy \\ + \;& \mu_2\int_\Omega \delta(\phi_2)|\nabla\phi_2|\,dx\,dy + \eta_2\int_\Omega H(\phi_2)\,dx\,dy \\ + \;& \tfrac{\beta}{4}\int_\Omega \Big(\big(|\nabla\phi_1|^2-1\big)^2+\big(|\nabla\phi_2|^2-1\big)^2\Big)\,dx\,dy \\ + \;& \tfrac{\alpha}{2}\int_\Omega \big(|\nabla\phi_1|^2+|\nabla\phi_2|^2\big)\,dx\,dy. \end{aligned} \tag{7}$$

Here the given image I is again a scalar function. In contrast with the two previous segmentation models, now ϕ is a vectorial function, $\phi=(\phi_1,\phi_2)$, *i.e.* there are two segmentation curves, the zero level sets of ϕ_1 and ϕ_2, which segment the image into four regions (inside both curves, inside one and outside the other, and outside both curves). Therefore the vector c has also four components, $c=(c_{11},c_{10},c_{01},c_{00})$ and the corresponding weighting parameters are now λ_{11}, λ_{10}, λ_{01} and λ_{00}. The functions H, δ, have the same interpretation as before, as well as, β, α and μ_j, η_j for $j=1,2$.

We remark that the vector-valued model (6) reduces to the scalar model (4), when all the components I_i are equal. Moreover, the scalar model (4) is also called a two-phase segmentation model (it segments the image into two disjoint regions), when compared to model (7), which divides the image into four different homogeneous regions. In addition, analogous formulas to (5), for the average vector c components in (6) and (7), can be derived (see [4, 27]).

In [3], it is shown that for each fixed c (and considering $\alpha=\beta=0$) the minimization problem $\min_\phi F(\phi,c)$, which is a non-convex minimization problem, can be equivalently reformulated as a convex unconstrained minimization problem. Using this idea, the numerical scheme we use to approximate the solution of the vector-valued segmentation model (3) is a two-step scheme, where in the first step the values of the unknown average region c are computed by means of the segmentation function ϕ (see (5)

for the scalar segmentation model (4)) and in the second step the minimization of $F(.,c)$ is performed updating the level set function ϕ. The procedure for solving this second step, involves a finite element discretization in space and then a Levenberg-Maquardt Newton-type optimization method (see [11] for more details: More exactly it is a combination of steepest descent, for robustness, and Newton, for quadratic convergence, methods).

3 Numerical experiments

We report now the experiments and results for the endoscopic images. For each image, which is a RGB image; *i.e.* $I = (I_R, I_G, I_B)$, we consider only the region enclosed by the black background area (see Figure 1, (b) and (c)). We have performed the following :

1. (a) The image I was converted into a gray-scale image $\overline{I}_{gs}$.
   (b) The image $\overline{I}_{gs}$ was smoothed, by using the heat equation $\frac{\partial u}{\partial t} - \triangle u = 0$ for $0 < t < T$ in a rectangular domain Ω with periodic boundary conditions. The initial condition $u(.,0)$ is set to the gray scale image $\overline{I}_{gs}$. The function I_{gs} is defined to be $u(x,T)$, i.e. the smoothed image.
   (c) The Gaussian curvature $\mathcal{K}$ and mean curvature $\mathcal{H}$ of I_{gs} were computed, as indicated in section 2.1, as well as, the product $\mathcal{P} = -\mathcal{K}\min(\mathcal{H}, 0)$.
2. Then, the segmentation procedures below were performed, for segmenting the image I:
   (a) The two-phase model (4) was applied to $\mathcal{P}$.
   (b) The vector-valued model (6) was applied directly to I.
   (c) The four-phase model (7) for the smoothed image I_{gs} was performed.

Remark 3.1 *We remark that other linear smoothing filters may be applied to obtain I_{gs}. However, since Total-Variation based filters have a tendency to create flat regions away from edges in the image, so these type of filters are not appropriate for our purposes – as the curvatures information will be destructed by such filters. In our approach, the time T determines the amount of smoothing which we apply to the given image. This is a parameter which one may experiment with in practice, depending on the noise level and the targeted polyps size relative to other features in the image.*

For one image (see Figure 6) a combination of the four-phase model (7) for I_{gs} and the two-phase model (4) for $\mathcal{K}$, were carried out. This combination was done in the following way: first the four-phase segmentation model for I_{gs} was performed. By analyzing the result we knew which was the curve, say ϕ_1, that segmented the polyp and the other, say ϕ_2, that segmented the mucosa and or the lumen. So to the former, ϕ_1, we "added" the two-phase segmentation of $\mathcal{K}$; this means we employed a four-phase segmentation for I_{gs}, where one curve was re-enforced with the two-phase segmentation of $\mathcal{K}$ (we emphasize that a four-phase segmentation model is a coupling of two segmentations, each one having two phases).

The computations in steps 1b and 1c were done with a square Cartesian grid (corresponding exactly to the size of the input grayscale image $\overline{I}_{gs}$) and MATLAB® [24] was used for the numerical implementation. In addition, for the segmentation models a finite element mesh with 100^2 elements was used to discretize the spatial domain. For the numerical implementation we used COMSOL MULTIPHYSICS® [6] (a software for solving partial differential equations using finite elements).

The Figure 3 provides in the first row the medical image (a) (containing a roundish polyp), the corresponding smoothed grayscale image I_{gs} in (d), and the curvature function $\mathcal{P}$ in (e). The subfigures (b), (c) and (f) show several segmentations superimposed on the medical image. (b) is the segmentation with the vector valued model (6) using the three color channels of the original image I. (c) shows the four-phase segmentation (see (7)) for I_{gs}. (f) illustrates the segmentation obtained with the two-phase model for $\mathcal{P}$. From this Figure 3, the four-phase segmentation of u is far superior to the segmentations

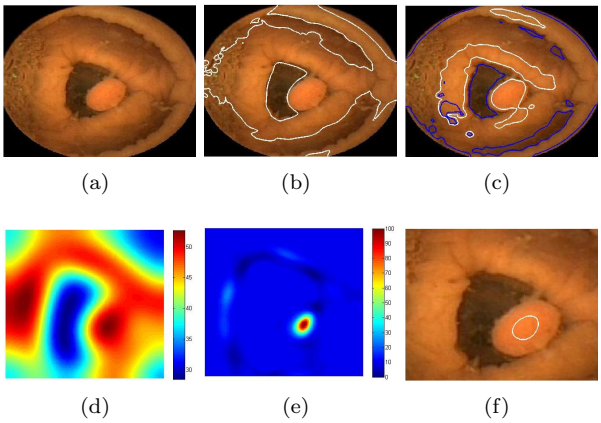

Figure 3: (a) Medical image (from RAPID 6 Atlas v3 of *Given Imaging*) showing a polyp, colonic folds and the lumen. (b) Vector valued RGB segmentation (white contours) of the original image I. (c) Four phase segmentation for I_{gs} (white and blue contours). (d) Cropped smoothed grayscale image I_{gs}. (e) Function $\mathcal{P}$ computed from (d). (f) Two-phase segmentation (white contour) of $\mathcal{P}$ superimposed to the medical image.

obtained with the vector-valued model, and the last segmentation in (f), involving the curvature function $\mathcal{P}$ clearly detects the polyp and segments its upper part.

The Figure 4 contains three medical images (a), (b) and (c) ((a) and (b) belong to the same PillCam colon video). Each one shows a polyp, with a roundish shape, and in (a) and (c) it is clearly attached to the colonic fold. All the polyps are covered by liquid and the dark region corresponds either to the lumen or trash liquid. The first column refers to medical image (a), the second to (b) and the third do (c). This Figure 4 reports the segmentation results (represented by the white contours in (j), (k), (l), (m), (n), (o) and the white and blue contours in (p), (q), (r)), as well as, the smoothed grayscale image I_{gs} (see (d), (e) and (f)) and information about geometric features (the curvature function $\mathcal{P}$ in (g), (h) and (i)). Again the polyp present in each medical image is perfectly detected using the function $\mathcal{P}$ (see (j), (k) and (l)).

The Figure 5 lists four medical images, in the first column, each one showing a roundish poly, which is detected by the two-phase segmentation of the curvature function $\mathcal{P}$ (white curve in (a), (e), (i), (m)). Each row contains four images, which represent (from left to right): the original medical image (cropped image for (i)) with the segmented polyp (white contours), the function $\mathcal{P}$ computed over the smoothed gray-scale image I_{gs}, the vector valued RGB segmentation of the original image I, the four phase segmentation of I_{gs}. As we can see, the vector valued RGB segmentation is already good, but the four-phase segmentation of I_{gs} is even better (it gives a correct segmentation of the lumen (orifice of the colon), as well as, colonic mucosa and polyp). However, the two-phase segmentation of the curvature function $\mathcal{P}$, is even better because it accurately singles out the polyp in the image.

The Figure 6 shows a sessile poly in (a) (on the right). In the first row, (b), (c) and (d) present, respectively, the smoothed gray-scale image I_{gs}, the smoothed Gaussian curvature $\mathcal{K}$ (obtained by using the heat equation as described in 1b), and the function $\mathcal{P}$. As it can be seen, this latter function has almost no information about the poly, whereas $\mathcal{K}$ has some meaningful and important information concerning the polyp location and shape. The sub-figure (g) demonstrates the successful segmentation obtained with the two-phase model, applied to the single smoothed Gaussian curvature $\mathcal{K}$. Also in sub-figure (h), which shows the result of the combined four-phase model for I_{gs} with the two-phase model for $\mathcal{K}$, displays and acceptable segmentation, that detects the polyp. The vector-valued model, using the RGB channels, completely fails to detect the poly (see (e)), as well as, the four-phase model for the smoothed gray-scale image I_{gs} (see (f)).

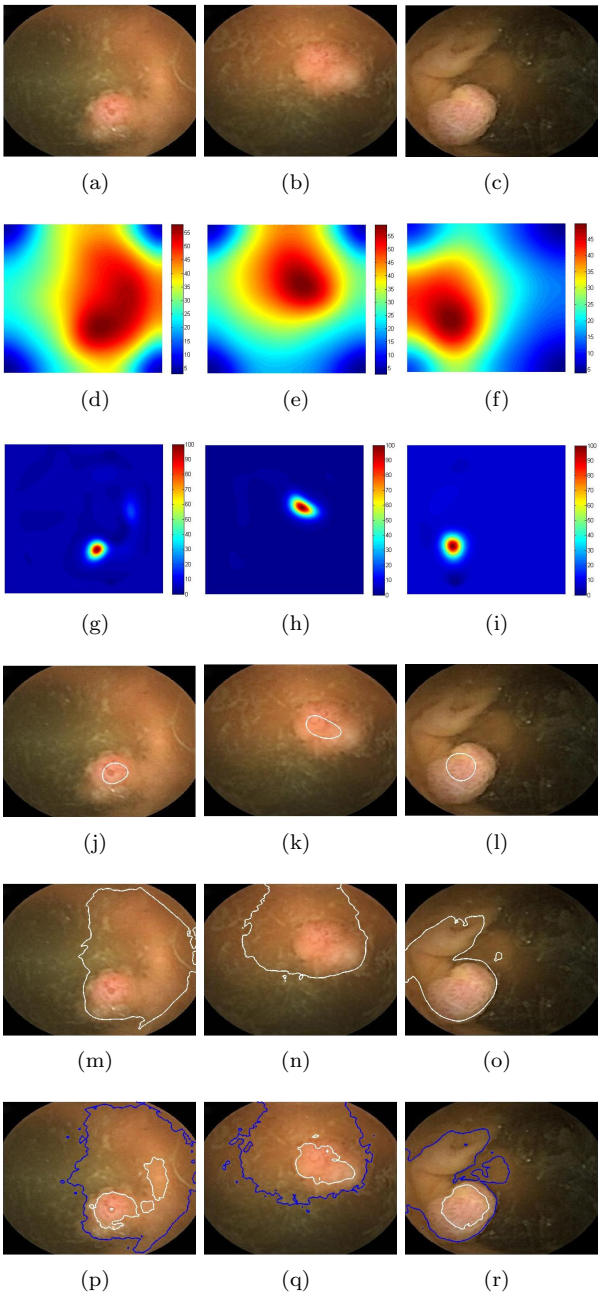

Figure 4: First row: Three medical images (Department of Gastroenterology, University Hospital of Coimbra) with polyps (a), (b) and (c). Second row: Smoothed grayscale images I_{gs}. Third row: Function $\mathcal{P}$ computed from (d), (e) and (f). Fourth row: Two-phase segmentation (white contours) of $\mathcal{P}$ superimposed to the medical image. Fifth row: Vector valued RGB segmentations (white contours) of the original images I. Sixth row: Four phase segmentations for the smoothed grayscale image I_{gs} (white and blue contours).

We point out that for this image shown in Figure 6 (a), before smoothing the Gaussian curvature $\mathcal{K}$, we first defined a threshold s for $\mathcal{K}$, and in the points (x, y), where $\mathcal{K}(x, y) > s$ we redefined $\mathcal{K}(x, y)$ to

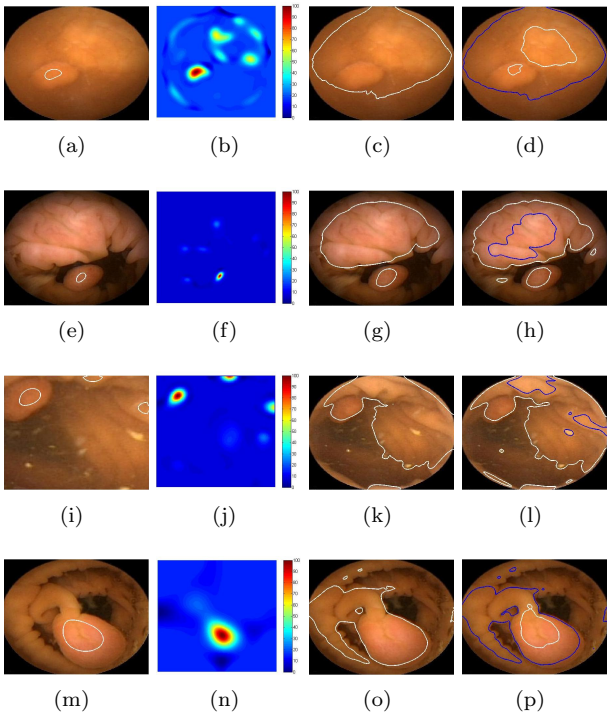

Figure 5: First column: four medical images (from RAPID 6 Atlas v3 of *Given Imaging*) with the two-phase segmentations of function $\mathcal{P}$ superimposed (white contour detecting the polyp). Second column: the function $\mathcal{P}$. Third column: the vector valued RGB segmentations of the original image I. Fourth column: the four phase segmentation of I_{gs}.

be the average of the values of $\mathcal{K}$ in a small neighborhood centered at the point (x, y). In effect, and similarly to the synthetic structures exhibited in Figure 2, the Gaussian curvature has big discontinuities, and sometimes in the colonic folds the Gaussian curvature reaches very high values, interfering with the values of the Gaussian curvature of the polyp itself.

The recent second-generation capsule endoscopy system, PillCam Colon 2 (released at the end of 2009), was developed for improving the PillCam Colon system characteristics. Moreover, a multicenter performance evaluation [9] shows the effectiveness of PillCam Colon 2 capsule on a spectrum of colonic lesions. The images from the second-generation capsules exhibit better resolution and less noise, and the geometric characters of the underlying surfaces seem to be the same. Therefore, we expect that our proposed algorithm applies to the images acquired by these new capsules as well. In Figure 7 we show the results of our method applied to two images (they are the first and fourth images displayed in the first row of Figure 3, page 1030, of [9]) taken by this second generation capsule. As it can be seen, again the proposed curvature based methodology works well, and give a good localization of polyps (marked by the red regions) in sub-figures (b) and (d).

4 Comments and future work

In this paper automatic detection of colonic polyps in wireless capsule endoscopic images has been carried out. This analysis has concentrated on geometric and "image intensity" features of the input medical image, together with variational segmentation techniques. We demonstrated that geometrical characterization of the polyps can lead to very effective identification from the capsule images. This geometrical characterization can easily be computed by simple formulas involving Gaussian and the mean curvature.

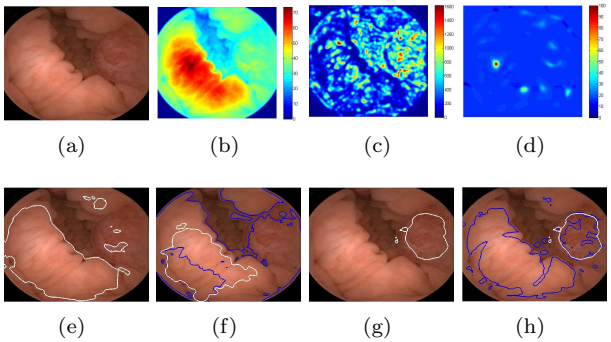

Figure 6: (a) Medical image (Department of Gastroenterology, University Hospital of Coimbra) with a sessile polyp on the right side. (b) Smoothed gray-scale image I_{gs}. (c) Smoothed Gaussian curvature $\mathcal{K}$. (d) Function $\mathcal{P}$. (e) Vector valued RGB segmentation of the original image I. (f) Four phase segmentation for the smoothed grayscale image I_{gs}. (g) Two-phase segmentation using the single smoothed Gaussian curvature $\mathcal{K}$. (h) Four phase segmentation for I_{gs} combined with a two phase segmentation for $\mathcal{K}$.

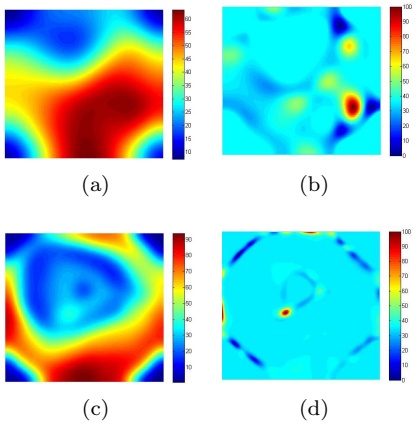

Figure 7: Results of our method applied to images from PillCam Colon 2. First column (a) and (c): smoothed gray-scale images I_{gs} of the first and fourth medical images displayed in the first row of Figure 3, page 1030, of [9]. Second column (b) and (d): Functions $\mathcal{P}$ computed from (a) and (c) – the red regions indicate the polyps.

On the whole, the results indicate a good performance of these variational schemes. For all the images the segmentation of a function depending either on both the Gaussian and mean curvatures (see Figures 3, 4, 5, 7), or only the Gaussian curvature (see Figure 6), was the only way to single out the polyp. For some images (see Figures 3, 4, 5), the RGB segmentation of the original image gave acceptable results (concerning the lumen (orifice of the colon) and colonic mucosa), although inferior to the four-phase segmentation of the smoothed gray-scale input image. It is also important to emphasize that for some images (see for instance Figure 5) the four-phase segmentation gave already a good segmentation of the polyp (though, in general, the polyp is not singled out, it rather appears as part of the colonic mucosa segmentation).

For one image (see Figure 6) the segmentation of the Gaussian curvature, was the only way to detect the polyp. Also, in this same image, the segmentation of the Gaussian curvature when combined with the four-phase segmentation of the smoothed gray-scale input image improved the result. However, we point out here that the polyp in this image barely satisfies (at least from the image) our assumptions on

the geometries.

The main approach proposed in this paper, which relies on the segmentation of the curvature based function $\mathcal{P}$, seems to correctly locate and detect the colonic polyps (exhibiting a cap-like structure with no stalk) in wireless capsule images. Though it does not lead to a complete segmentation, because only the higher part of the polyp, is in general detected. However we believe that the detection of the polyp is, by itself, a good result, and furthermore this is a fully automatic process.

In the future we intend to generalize the methodology described in this paper to video images. In this case, very efficient multi-phase segmentation algorithms may be needed. We plan to investigate if the fast algorithms of [10] may be of use in this project. In addition we will also analyze, further, the geometric information provided in the images, and try to overcome the above mentioned issue related to a complete segmentation of the whole polyp. Furthermore, we plan to conduct extensive experiments for a data-base set of wireless endoscopic images, that we have at our disposal in the Department of Gastroenterology, of the University Hospital of Coimbra.

Acknowledgments

This work is partially supported by Contract UTAustin/MAT/0009/2008 from the UT Austin | Portugal Program (http://www.utaustinportugal.org/). The third author is also partially supported by: National Science Foundation DMS-0914465, DMS-0914840, and a MURI sub-contract from Univ. of S. Carolina grant No. W911NF-07-1-0185.

References

[1] D. G. Adler and C. J. Gostout. Wireless capsule endoscopy. *Hospital Physician*, pages 16–22, 2003.

[2] J. Berens, M. Mackiewicz, and D. Bell. Stomach, intestine and colon tissue discriminators for wireless capsule endoscopy images. In *SPIE Conference on Medical Imaging*, pages 283–290, Austria, 2005. vol. 5747.

[3] T. F. Chan, S. Esedoḡlu, and M. Nikolova. Algorithms for finding global minimizers of image segmentation and denoising models. *SIAM Journal of Applied Mathematics*, 66(5):1632–1648, 2006.

[4] T. F. Chan, B. Y. Sandberg, and L. A. Vese. Active contours without edges for vector-valued images. *Journal of Visual Communication and Image Representation*, 11(2):130–141, 2000.

[5] T. F. Chan and L. A. Vese. Active contours without edges. *IEEE Transactions on Image Processing*, 10(2):266–277, 2001.

[6] Comsol Multiphysics®. *http://www.comsol.com/*.

[7] R. Dahyot, F. Vilarino, and G. Lacey. Improving the quality of color colonoscopy videos. *EURASIP Journal on Image and Video Processing*, pages 167–188, 2008. Article ID 139429, 7 pages.

[8] M. Delvaux and G. Gay. Capsule endoscopy: Technique and indications. *Best Practice & Research Clinical Gastroenterology*, 22(5):813–837, 2008.

[9] R. Eliakim, K. Yassin, Y. Niv, Y. Metzger, J. Lachter, E.Gal, B. Sapoznikov, F. Konikoff, G. Leichtmann, Z. Fireman, Y. Kopelman, and S. N. Adler. Prospective multicenter performance evaluation of the second-generation colon capsule compared with colonoscopy. *Endoscopy*, 41(12):1026–1031, 2009.

[10] Selim Esedoḡlu and Yen-Hsi Richard Tsai. Threshold dynamics for the piecewise constant Mumford-Shah functional. *J. Comput. Phys.*, 211(1):367–384, 2006.

[11] I. N. Figueiredo, P. N. Figueiredo, G. Stadler, O. Ghattas, and A. Araújo. Variational image segmentation for endoscopic human colonic aberrant crypt foci. *IEEE Transactions on Medical Imaging*, 29(4):998–1011, 2010.

[12] J. Gerber, MPhil ARCS, Ari Bergwerk, and David Fleischer. A capsule endoscopy guide for the practicing clinician: technology and troubleshooting. *Gastroentestinal endoscopy*, 66(6):1188–1195, 2007.

[13] S. B. Gokturk, C. Tomasi, A. Burak, C. F. Beaulieu, D. S. Paik, R. B. Jeffrey Jr, J. Yee, and S. Napel. A statistical 3-D pattern processing method for computer-aided detecting of polyps in CT colonography. *IEEE Transaction on Medical Imaging*, 20(12):1251–1260, 2001.

[14] D.K. Iakovidis and D.E. Maroulis. A comparative study of texture features for the discrimination of gastric polyps in endoscopic video. In *18th IEEE Symposium on Computer-based Medical System*, 2005.

[15] G. Iddan, G. Meron, A. Glukhovsky, and F. Swain. Wireless capsule endoscopy. *Nature*, 405(6785):417, 2000.

[16] A. Moglia, A. Menciassi, and P. Dario. Recent patents on wireless capsule endoscopy. *Recent Patents on Biomedical Engineering*, 1(1):24–33, 2008.

[17] A. Moglia, A. Menciassi, P. Dario, and A. Cuschieri. Capsule endoscopy: progress update and challenges ahead. *Nature Reviews Gastroenterology and Hepatology*, 6:353–361, 2009.

[18] T. Nakamura and A. Terano. Capsule endoscopy: past, present, and future. *Journal of Gastroenterology*, 43:93–99, 2008.

[19] S. Osher and R. Fedkiw. *Level set methods and dynamic implicit surfaces*. Springer-Verlag, New York, NY, USA, 2003.

[20] S. Osher and J. A. Sethian. Fronts propagating with curvature-dependent speed: algorithms based on hamilton-jacobi formulations. *Journal of Computational Physics*, 79(1):12–49, 1988.

[21] D. S. Paik, C. F. Beaulieu, G. D. Rubin, B. Acar, R. B. Jeffrey Jr, J. Yee, J. Dey, and S. Napel. Surface normal overlap: A computer-aided detection algorithm with application to colonic polyps and lung nodules in helical CT. *IEEE Transactions on Pattern Analysis and Machine Intelligence*, 23(6):661–675, 2004.

[22] J.P. Silva Cunha, M. Coimbra, P. Campos, and J.M. Soares. Automated topographic segmentation and transit time estimation in endoscopic capsule exams. *IEEE Transactions on Medical Imaging*, 27(1):19–27, 2008.

[23] R. M. Summers, C. D. Johnson, L. M. Pusanik, J. D. Malley, A. M. Youssef, and J. E. Reed. Automated polyp detection at CT colonography: Feasibility assessment in a human population. *Radiology*, 219:51–59, 2001.

[24] The Mathworks, Inc. *http://www.matlab.com.*

[25] P-S Tsai and M. Shah. Shape from shading using linear approximation. *Image and Vision Computing*, 12(8):487–498, 1994.

[26] C. van Wijk, V. F. van Ravesteijn, F. M. Vos, and L. J. van Vliet. Detection and segmentation of colonic polyps on implicit isosurfaces by second principal curvature flow. *IEEE Transactions on Medical Imaging*, 29(3):688–698, 2010.

[27] L. Vese and T. F. Chan. A multiphase level set framework for image segmentation using the mumford and shah model. *International Journal of Computer Vision*, 50(3):271–293, 2002.

[28] G. H. Wang, J. Q. Han, and X. M. Zhang. Three-dimensional reconstruction of endoscope images by a fast shape from shading method. *Measurement Science and Technology*, 20, 2009.

[29] C. Wu, S. G. Narasimhan, and B. Jaramaz. A multi-image shape-from-shading framework for near-lighting perspective endoscopes. *International Journal of Computer Vision*, 86:211–228, 2010.

[30] J. Meng Y. Jiang, , and N. Jaffer. A novel segmentation and navigation method for polyps detection using mathematical morphology and active contour models. In *6th IEEE International Conference on Cognitive Informatics*, pages 357–363, 2007. D. Zhang, Y. Wang, and W. Kinsner (Eds.).

[31] H. Yoshida and J. Nappi. Three-dimensional computer-aided diagnosis scheme for detection of colonic polyps. *IEEE Transactions on Medical Imaging*, 20(12):1261–1274, 2001.